

Structure, thermodynamic, and transport properties of molten Mg_2SiO_4 : Molecular dynamics simulations and model EOS

G. BEN MARTIN,^{1,*} FRANK J. SPERA,¹ MARK S. GHIORSO,² AND DEAN NEVINS¹

¹Department of Earth Science, University of California-Santa Barbara, Santa Barbara, California 93101, U.S.A.

²OFM-Research Inc., 7336 24th Avenue, NE, Seattle, Washington 98115, U.S.A.

ABSTRACT

Molecular dynamics simulations have been used to study the structure, equation of state (EOS), self-diffusion, and shear viscosity of molten Mg_2SiO_4 for pressures and temperatures in the range 2.5–110 GPa and 2100–5060 K, respectively. The transferable pair-potential parameters of Matsui (1998) for the system $\text{Na}_2\text{O-CaO-MgO-Al}_2\text{O-SiO}_2$ have been used accounting for Coulomb, Born, and van der Waals forces. Simulations have been carried out in the microcanonical (NEV) ensemble at 63 state points along 12 isochores spanning the density range 2754–4500 kg/m^3 . Thermodynamic properties including the isochoric heat capacity, isobaric expansivity, isothermal compressibility, thermal pressure, and the Grüneisen parameter (γ) are computed directly from MD results. A density crossover between molten Mg_2SiO_4 and forsterite crystals occurs at ~15 GPa at 2100 K. We find the Grüneisen parameter to be a function of temperature (T), increasing with increasing T at low density ($\rho < 3400 \text{ kg/m}^3$) but decreasing as T rises at high density ($\rho > 3400 \text{ kg/m}^3$); hence, the integrated form of the Mie-Grüneisen EOS is only approximately valid for liquid Mg_2SiO_4 since γ varies by ~20% over the T range along an isochore. Radial distribution functions for all atoms around all other atoms were used to generate coordination statistics as a function of pressure (P) and T . Oxygen about Si coordination increases from fourfold coordination at low pressure to sixfold at higher pressure; the abundance of distorted trigonal bipyramidal fivefold polyhedra, Si(V) maximizes at 30 GPa at 3500 K. Interestingly, O about O increases to a maximum of 13 at low P before decreasing with increasing pressure to ~10. The mean coordination number (CN) of Si around oxygen increases from 1.2 to 1.5 consistent with an increasing abundance of Si_2O_7 dimers as pressure increases. Self-diffusion of Mg, Si, and O was calculated at each state point giving activation energies of 67, 79, and 76 kJ/mol and activation volumes of 1.42, 1.10, and 1.32 cm^3/mol , respectively. Shear viscosity of the liquid calculated at 12 state points using the Green-Kubo formulation provides an excellent Arrhenian fit. Viscosity varies by a factor of ~20 ($1.5 \times 10^{-3} \text{ Pa s}$ to 0.03 Pa s) from 1 to 100 GPa. The validity of the Stokes-Einstein and Eyring expressions for atom mobility and shear viscosity is examined in detail. Characteristic lengths for atom mobility are consistent with ionic radii to within a factor of ~1.5–2 for all atoms. An equation of state and thermodynamic model for Mg_2SiO_4 liquid is developed consistent with the fundamental measure functional theory of Rosenfeld and Tarazona (1998). Our model reproduces the E - P - V - T relations and the derived thermodynamic properties obtained from the MD simulations to within the reported uncertainty.

Keywords: Forsterite liquid, equation of state, molecular dynamics, Grüneisen parameter, structure, viscosity, diffusion

INTRODUCTION

An understanding of the equation of state (EOS), atomic structure, and transport properties of molten silicates in geochemical systems is central to many aspects of planetary dynamics. Quantitative information bearing on the shear viscosity, self-diffusion coefficients, and thermal and ionic conductivities of molten silicates, including the relationship between atomic level structure and macroscopic property variation with pressure (P) and temperature (T), is indispensable in the analysis of geochemical processes. For example, understanding the cooling and crystallization of Earth's early magma ocean requires knowledge

of the thermodynamic and transport properties of MgO-rich silicate liquids at P and T in the range 0–135 GPa and 2000–6000 K, respectively. The state of the mantle following magma ocean solidification sets the initial conditions for growth and subsequent evolution of the lithosphere, continental and oceanic crust, the hydrosphere and the atmosphere, and impacts the start of subduction and the plate tectonic cycle on Earth (e.g., Anderson 2007). Because silicate liquids are generally more compressible than crystals of the same composition, a density crossover between magma and crystals might be anticipated at high pressure. It is possible, therefore, that crystalline olivine accumulated in a region of neutral buoyancy in the Earth's primitive magma ocean during and immediately following Earth accretion and Moon-forming impact. Arguments have been presented for the

* E-mail: gbenmartin@umail.ucsb.edu

presence today of regions of melt along the Earth's core-mantle boundary (Lay et al. 2004). Predictive models for the properties of multicomponent silicate melts are evidently useful for addressing various primary geochemical problems.

In addition to its importance in geoscience problems, an understanding of the amorphous state (liquid and glass), specifically the relationship between structure, the EOS, and transport properties, is of intrinsic interest in its own right. Liquid-liquid phase separations in which two liquids of distinct composition coexist are common in multicomponent natural systems (e.g., Roedder 1951; Philpotts 1976). There is now growing interest in a more unusual situation of polyamorphism, a phenomenon whereby a one-component system can exist with at least two liquid or amorphous phases having the same chemical composition but distinct densities. Phase transitions between liquids occur without change in composition but instead with a change in density as T or P are varied (Tanaka 2000). Experimental evidence for polyamorphism has been found in several systems including molten silica, H_2O , and binary melts in the system $\text{Al}_2\text{O}_3\text{-Y}_2\text{O}_3$ (Aasland and MacMillan 1994; Senker and Rossler 2001; De-benedetti 1996). The existence or lack of polyamorphism can be predicted from critical point analysis of the thermodynamic EOS. Molecular dynamics (MD) simulation has proved to be a useful tool for searching for possible liquid-liquid phase transitions in silicate melts (Saika-Voivod et al. 2000; Skibinsky et al. 2004). Here we extend this search to molten Mg_2SiO_4 by performing a sufficient number of MD simulations to enable accurate derivation of its EOS to assess polyamorphism. Many additional aspects of the liquid state remain to be explored. Most significant to geochemical systems is the profound reorganization of melt structure upon pressure increase. Atomic-level structural modifications exert a first-order influence on the melt properties that, in turn, play important geodynamical roles. A better understanding of the liquid state is clearly applicable to many important geodynamical issues.

In this study, the structure and properties of liquid Mg_2SiO_4 at elevated P and T are computed by MD simulation and compared to laboratory results. Additionally, the MD-derived data are used to build comprehensive expressions for the EOS, internal energy, and related thermodynamic properties of liquid Mg_2SiO_4 and to investigate the possibility of a liquid-liquid phase transition. The transferable pair-potential model of Matsui (1998) for the system $\text{Na}_2\text{O-CaO-MgO-Al}_2\text{O}_3\text{-SiO}_2$ is used to study liquid Mg_2SiO_4 at density (ρ), T , and P in the range 2754–4500 kg/m^3 , 2100–5000 K, and 2–110 GPa, respectively. The properties of liquid Mg_2SiO_4 have been computed at 63 state points along 12 isochores utilizing 50 picoseconds (ps) duration equilibrium or metastable liquid MD simulations. A first nearest neighbor analysis of Mg, Si, and O as a function of density (pressure) along several isotherms is presented. Thermodynamic parameters including the isochoric heat capacity, the Grüneisen parameter, the isothermal compressibility and isobaric expansivity are presented later at all of the state points studied. Self-diffusivities of Mg, Si, and O are used to compute activation energies and volumes, and the connection between self-diffusion and short-range melt structure is elucidated. In addition, 12 “long-duration” MD simulations of 2 nanoseconds (ns) were made to compute the shear viscosity by the Green-Kubo method as a function of temperature and

pressure. These long-duration simulations enable a test of the applicability of the Stokes-Einstein and Eyring relations between self-diffusivity of Mg, Si, and O and melt shear viscosity and afford a comparison between the activation energy and volumes for self-diffusion and viscous flow.

MOLECULAR DYNAMICS SIMULATIONS: POTENTIALS AND COMPUTATIONAL DETAILS

A description of the MD method with details regarding the implementation and protocol used in this study may be found in Nevins (2009). Here we briefly present relevant details pertinent to Mg_2SiO_4 liquid. The potential used in this study is the semi-empirical pair potential of Matsui (1998) for the system $\text{Na}_2\text{O-CaO-MgO-Al}_2\text{O}_3\text{-SiO}_2$. The functional form of the potential includes contributions from long-range Coulombic forces, short-range Born-Mayer exponential repulsion and van der Waals dipolar attractive forces. The potential between two atoms i - j is:

$$\Phi_{ij}(r_{ij}) = \frac{q_i q_j e^2}{4\pi\epsilon_0 r_{ij}} + A_{ij} \exp\left(-\frac{r_{ij}}{B_{ij}}\right) - \frac{C_{ij}}{r_{ij}^6} \quad (1)$$

where ϵ_0 is the permittivity of free space, r_{ij} is the distance between atoms i and j , q_i is the charge of the i^{th} atom, and A_{ij} , B_{ij} , and C_{ij} are parameters that quantify the short-range energetics of atom pair ij . Figure 1 shows the potential energy as a function of interatomic distance (r) for Mg-O, Si-O, and O-O interactions. The potential form is radially symmetric and pairwise additive. Fractional charges are used in the MD simulations, with $q_{\text{O}} = -0.945$, $q_{\text{Mg}} = 0.945$, and $q_{\text{Si}} = 1.89$. The parameters used to define the potential energy interactions are given in Table 1. Details on how the potential was derived may be found in Matsui (1998).

Molecular dynamics simulations were performed using 8001 atoms (1143 formula units) in the microcanonical (NEV) ensemble. Each MD run followed the same protocol: (1) initial positions were configured with atoms in random positions; (2) the system was run at a fixed temperature of 10 000 K for 2 ps to remove excess energy; (3) the resulting configuration was run for 2 ps to stabilize following removal of residual net momentum; (4) the system was then cooled to the desired temperature using velocity scaling for 12 ps; and (5) finally, a 50 ps production simulation was carried out on the equilibrium liquid. Steps 2–5 were run using a timestep of 1 femtosecond (fs). All simulations were carried out at fixed volume (density). To verify that thermal equilibrium was achieved for each 50 ps production run, the average simulation temperature was computed for the first and last 10 ps of each 50 ps production run. The two temperature

TABLE 1. Parameters used to define the potential energy pairwise interactions given in text Equation 1

Atom pair	A (kJ/mol)	B (nm)	C [(kJ·nm ⁶)/mol]
Mg-Mg	1.70E+09	0.80	8.44E-04
Mg-Si	3.55E+10	0.63	1.43E-03
Mg-O	3.14E+06	1.78	2.63E-03
Si-Si	7.71E+12	0.46	2.43E-03
Si-O	4.84E+06	1.61	4.47E-03
O-O	6.24E+05	2.76	8.21E-0

Notes: The values are from Matsui (1998).

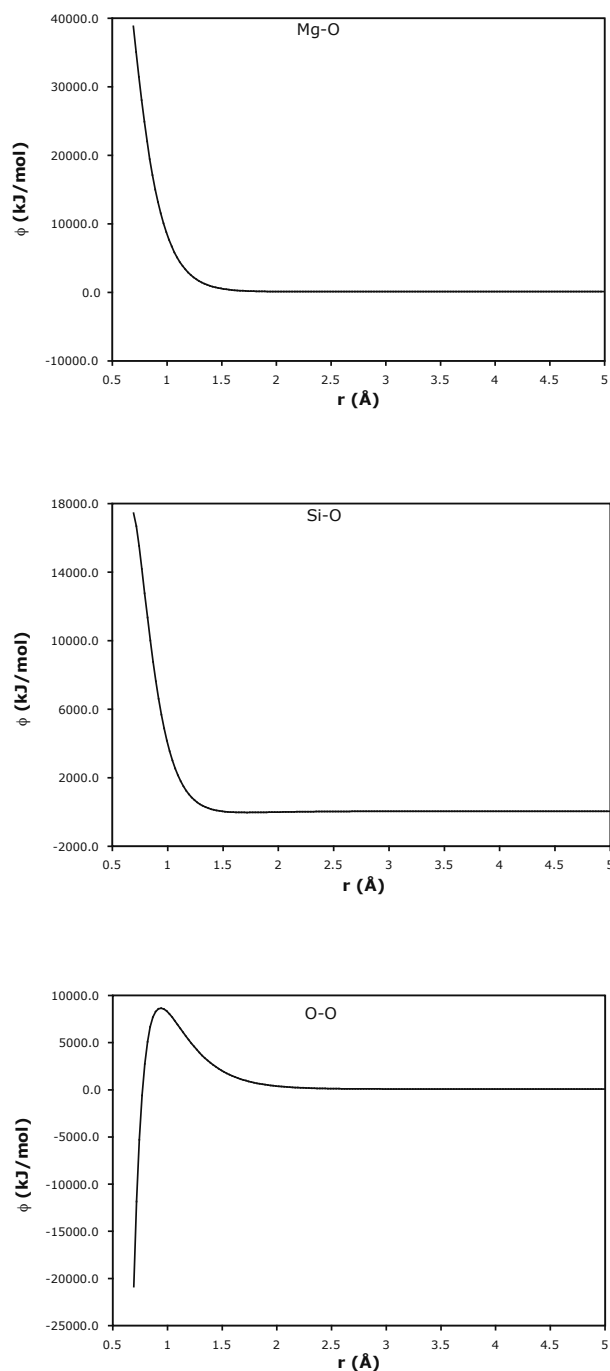


FIGURE 1. Interatomic potentials for Mg-O, Si-O, and O-O pair interactions. The form of the potential is given by Equation 1 in text; numerical parameters given in Table 1 are from Matsui (1998).

averages were always within the intrinsic temperature fluctuation of the specified simulation (σ_T), in fact usually much closer (3–5 K). Atom trajectories were saved at 10 fs intervals as was T , P , kinetic energy (U_K), isochoric heat capacity (C_V), and potential energy (U_P). The fluctuations in temperature (σ_T) and pressure (σ_P) due to the finite size system were calculated at the end of each run. Fluctuation theory informs us that σ_T and σ_P scale as

$N^{-1/2}$ where N is the number of atoms used in the simulation (McQuarrie 2000). The $N^{-1/2}$ scaling implies, for example, that σ_T and σ_P are four times smaller in a MD simulation of 8000 atoms compared to one with 500. Using too small an N introduces unacceptable uncertainties in MD state point coordinates (P and T) and directly propagates into uncertainties in thermodynamic and transport properties and into structural states defined by nearest neighbor coordination statistics. The fluctuations for each run are gathered in Table 2¹; typically, σ_T is ~ 25 K and σ_P is ~ 0.25 GPa. These values represent the intrinsic uncertainty to all state points in this study given the potential parameters of Table 1. Note that these uncertainties are generally smaller than those of many laboratory experiments at the conditions of elevated T and P explored in this study.

RESULTS

Thermodynamic properties

The essential results for each equilibrium simulation are presented in Tables 2¹ and 3¹. Figure 2 gives the location in P - T coordinates of 63 state points along the 12 isochores studied. Because study of phase relations was beyond the scope of this paper, we used the fusion curve of Ghiorso (2004) to demonstrate that most of the state points simulated here were within the liquid field determined by other studies. Points below the fusion curve are in the metastable liquid range. The isochores

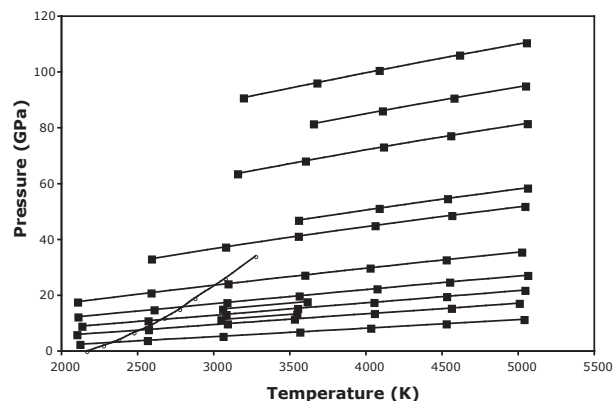


FIGURE 2. Location of state points in P - T space investigated by MD simulation in this study. State point uncertainties are identical to T and P fluctuations of $\sigma_T \approx 25$ K and $\sigma_P \approx 0.25$ GPa, respectively. The fusion curve of forsterite is from Ghiorso (2004). Most of the simulations are in the equilibrium liquid field although a few correspond to metastable liquid.

¹ Deposit item AM-09-023, Tables 2 and 3 (essential results for each equilibrium simulation), and Appendix (thermodynamic relations and Equation of State) that includes Appendix Tables 1, 2, and 3 (data regarding the Rosenfeld-Tarazona functions and the Universal EOS) and Appendix Figures 1, 2, and 3. Deposit items are available two ways: For a paper copy contact the Business Office of the Mineralogical Society of America (see inside front cover of recent issue) for price information. For an electronic copy visit the MSA web site at <http://www.minsocam.org>, go to the American Mineralogist Contents, find the table of contents for the specific volume/issue wanted, and then click on the deposit link there.

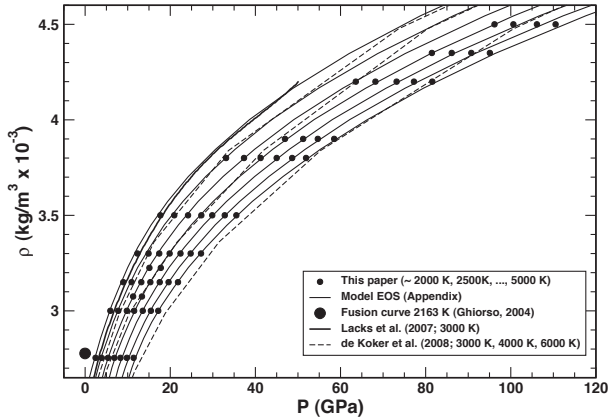


FIGURE 3. Density estimates for Mg_2SiO_4 liquid. State points computed in this paper are plotted as solid circles. The thin solid curves interpolate and extrapolate these state points using the EOS developed in the Appendix. The results of this paper are compared to the empirical potential MD calculations of Lacks et al. (2007; heavy solid curve) and the DFT MD estimates along three isotherms reported by de Koker et al. (2008). The large circle symbol indicates a zero pressure estimate of the molar volume of Mg_2SiO_4 liquid calculated from the initial slope of the forsterite fusion curve (Ghiorso 2004).

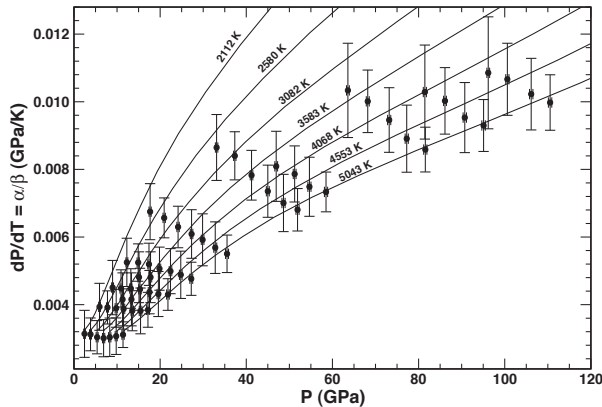


FIGURE 4. Thermal pressure coefficient (α/β) plotted vs. pressure. MD simulation data are shown with estimated uncertainties. Curves are calculated from the model developed in the appendix. Isotherms are chosen as average temperatures of the simulations.

are very slightly non-parallel implying there is a weak density (or pressure) dependence of the thermal pressure (see below). In the Appendix¹ we develop an EOS and thermodynamic model from the U - P - ρ state point data. Below, we evaluate some of the important thermodynamic quantities that may be derived from the MD simulation results.

The ρ - P - T results are re-plotted in Figure 3 to demonstrate the density variation with respect to pressure along the seven isotherms studied. These data points are interpolated and extrapolated by the EOS developed in the Appendix¹ as shown. Our results are offset to higher pressures with respect to the empirical potential MD simulations of Lacks et al. (2007) and

Belonoshko and Dubrovinsky (1996; not shown). Within the error of the density functional theory (DFT) MD results of de Koker et al. (2008), our state points are in agreement at low P , and systematically displaced to higher pressures at elevated P . All of the MD results shown in Figure 3 are in disagreement with the zero pressure volume of Mg_2SiO_4 liquid inferred from the analysis of the fusion curve, as estimated by Ghiorso (2004).

Thermal pressure. The near-linearity of the P - T coordinates on Figure 2 implies that the thermal pressure, $(\partial\rho/\partial T)_V = \alpha/\beta = \alpha K$, where α is the isobaric expansivity, $\alpha \equiv -\rho^{-1}(\partial\rho/\partial T)_P$, β is the isothermal compressibility, $\beta \equiv -\rho^{-1}(\partial\rho/\partial T)_T$, and K is the bulk modulus, is nearly constant along an isochore. Values of the thermal pressure were computed by centered finite difference methods at interior points and by backward and forward finite difference at the extremes. These values are presented in Table 3¹ and illustrated in Figure 4. The thermal pressure varies by about a factor of three from ~ 0.003 GPa/K at low density (2754 kg/m^3) to ~ 0.01 GPa/K at high density (4500 kg/m^3).

Isothermal compressibility and isobaric expansivity. Because the temperatures at which simulations were carried out along each isochore are the same within the temperature fluctuation, σ_T , the isothermal compressibility can be estimated at each state point. Finite difference methods were used to compute β (P, T) at each state point from its definition. Values are collected in Table 3¹. Values decrease along isochores as T and P increase. Along a low-density isochore (e.g., $\rho = 2754$ kg/m^3), β decreases by a factor ~ 2 as T and P increase ($2100 \rightarrow 5040$ K and $2 \rightarrow 11$ GPa, respectively) giving an isothermal bulk modulus ($K = \beta^{-1}$) of ~ 40 to ~ 65 GPa. The value of K at high melt density [$T \in (3200 \rightarrow 5053$ K), $P \in (90 \rightarrow 110$ GPa)] is ~ 470 GPa, 10 times that of the low- P value. For comparison, the isentropic bulk modulus of forsterite crystals at standard temperature and pressure (STP) is 128.2 GPa (Poirier 2000).

Combining values of the thermal pressure with those of the isothermal compressibility permits computation of the isobaric expansivity at each state point. Values of α (P, T) are collected in Table 3¹. The isobaric expansivity is larger at low T and P and decrease monotonically along isochores in response to increasing P and T . Values of the expansivity vary from 8×10^{-5} K^{-1} to 2.1×10^{-5} K^{-1} from lowest to highest P - T conditions; a typical representative value for liquid Mg_2SiO_4 is $\sim 4.5 \times 10^{-5}$ K^{-1} . In comparison, for forsterite crystals, $\alpha = 2.5 \times 10^{-5}$ K^{-1} at comparable P - T conditions (Poirier 2000).

Density inversion. Although the density of molten Mg_2SiO_4 is less than that of crystalline forsterite at low pressure, the compressibility of Mg_2SiO_4 liquid, like most liquids, exceeds that of its crystalline counterpart. This implies the possibility of a density inversion at high pressure where the density of forsterite is less than the density of liquid of identical composition. In such a case, olivine crystals will float in Mg_2SiO_4 liquid. In Figure 5, the density of crystalline forsterite based on the Vinet EOS determined by Ghiorso (2004) and liquid Mg_2SiO_4 from the MD simulations is shown along several isotherms. Although comparing our model to the Vinet EOS for the crystalline Mg_2SiO_4 is not self-consistent evidence for a density inversion since we have not used the Matsui potential to model crystalline forsterite, it does nevertheless suggest that a density crossover is a possibility.

In Figure 5a, at 2100 K, density inversion occurs at ~ 15

GPa equivalent to a depth on Earth of 430 km near the top of the transition zone region. At higher temperature, the neutral buoyancy depth increases; in Figure 5c, for example, at 3585 K the neutral buoyancy depth is ~35 GPa. Shock-wave studies of liquid Mg₂SiO₄ conducted by Mosenfelder et al. (2007) imply a density inversion at ~16 GPa, although the temperature of the shocked liquid was not given by these authors.

Internal energy. Energies are computed at each time step and the average for each run is given in Table 2¹. The kinetic energy of a classical ionic material in the high-temperature limit is $U_k = (3/2) nRT$, where R is the universal gas constant, and n is the number of atoms in the formula unit ($n = 7$). The MD-

computed values for U_k are within 1% of the classical limiting value, and this is not surprising considering the temperatures of the simulations.

Isochoric heat capacity and the Grüneisen parameter. The C_V was computed using centered finite differences to estimate the derivative:

$$C_V \equiv \left(\frac{\partial E}{\partial T} \right)_V.$$

Isochoric molar heat capacity values lay between 177 and 225 J/(mol·K) with an average of 200 J/(mol·K) over the P - T range of the simulations. The mean value can be compared to the extrapolated value for the isobaric molar heat capacity of forsterite crystals of 206 J/(mol·K) (Poirier 2000). Using the heat capacity in combination with the isothermal compressibility and isobaric expansivity, the Grüneisen parameter (γ) is computed from its definition:

$$\gamma = \frac{\alpha V}{\beta C_V}.$$

Values are given in Table 3¹. Using these values, the validity of the empirical power-law expression $\gamma = \gamma_0(\rho/\rho_0)^q$ relating the Grüneisen parameter to the melt density (e.g., Birch 1952; Anderson 1979; Quareni and Mulargia 1988) can be tested. Using simulation MF-1 for reference conditions, the fit gives $q = 1.29$ and $\gamma_0 = 0.86$ ($R^2 = 0.96$). At STP, forsterite crystals have $\gamma_0 = 1.18$ for comparison (Anderson 2007). Due mainly to the larger compressibility of liquid Mg₂SiO₄ compared to crystals, the reference Grüneisen parameter is somewhat smaller. Our values for the Grüneisen parameter fall within the limits of those measured for molten Mg₂SiO₄ by the shockwave experiments of Mosenfelder et al. (2007). For example, they found γ values ~0.4–1.2 at 3000 kg/m³ and 1.4–2 at 4500 kg/m³, whereas our results give a range of 0.88–1 and 1.43–1.57, respectively.

Finally, we can test the validity of the Mie-Grüneisen EOS. Recall that the thermal pressure is related to γ by the definition:

$$\left(\frac{\partial P}{\partial T} \right)_V = \gamma \frac{C_V}{V}. \quad (2)$$

Integrating at constant volume and assuming for the moment that γ is a constant, the Mie-Grüneisen EOS is obtained in the form:

$$P_2 - P_1 = \frac{\gamma}{V} \int_{T_1}^{T_2} C_V dT. \quad (3)$$

To apply this form of the Mie-Grüneisen EOS, the product $\gamma\rho$ must be constant along an isochore. In Figure 6, this quantity is plotted vs. pressure. In fact, there is a temperature dependence of $\gamma\rho$ such that for $\rho < 3400$ kg/m³, γ increases as T increases, whereas for $\rho > 3400$ kg/m³, the opposite holds. Quantitatively, there is a change of circa 15–20% in the product $\gamma\rho$ from 2000–5000 K. This change indicates that the simple form of the Mie-Grüneisen EOS is not adequate for modeling the high-temperature properties of liquid Mg₂SiO₄.

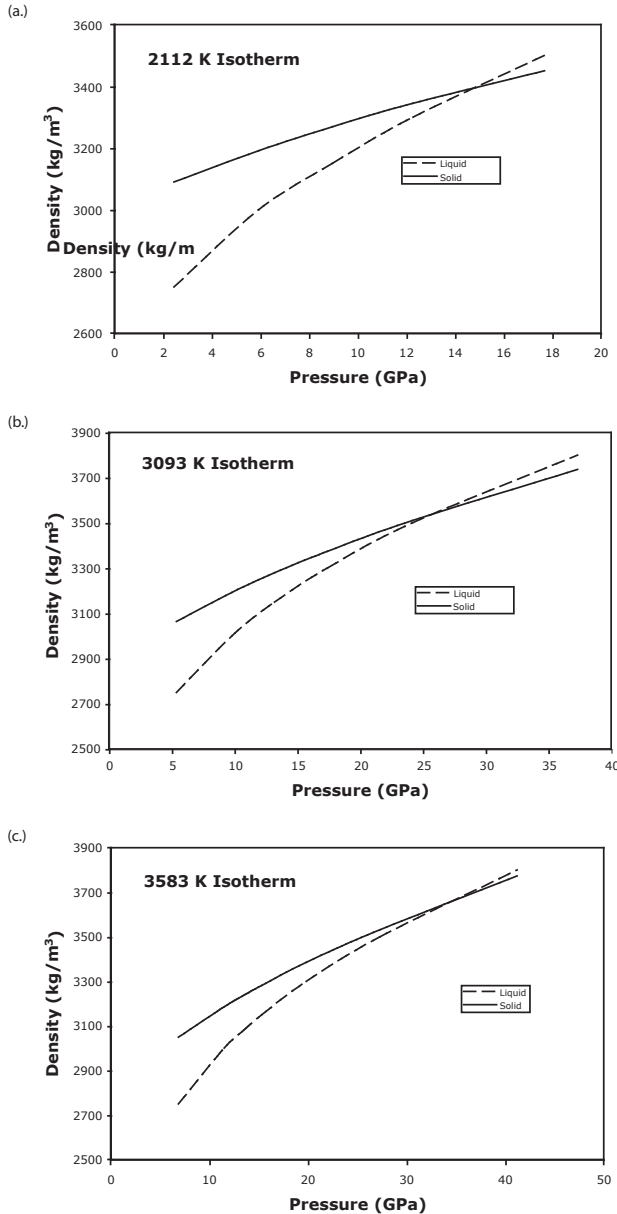


FIGURE 5. Density inversion, where the crystalline Mg₂SiO₄ becomes less dense than the liquid phase, shown for different temperatures.

Melt structure

Nearest neighbor coordination statistics. Melt structure and its variation with density (or pressure) and temperature can be investigated by examination of nearest neighbor coordination statistics or the coordination number (CN) of the i^{th} type of atom around every other type of atom j allowing for $i = j$. The CN of atom i around atom j (atom j is the central atom) is determined by first identifying for the pair the value of the radial coordinate r of the first minimum following the first maximum of the partial radial distribution function (RDF) $g_{ij}(r)$. The radial distribution function expresses the probability of finding a type i atom in a sphere of radius r around a type j atom. Because fluctuations in atom position are an intrinsic part of liquid behavior, many atom location “snapshots” are averaged to obtain robust CN statistics. In this study, approximately 50 000 snapshots are used to define the RDF for each CN analysis. The definition of the RDF:

$$g_{ij}(r) = \frac{1}{4\pi\rho r^2} \frac{d\langle N_{ij}(r) \rangle}{dr} \quad (4)$$

is used to determine $N_{ij}(r)$, average number of i atoms at a distance between r and $r + dr$ from atom j . Once the distance to the first minimum of the RDF is known, the CN is calculated by averaging position “snapshots” at 0.5 ps intervals. The averaging intervals were spaced by 0.5 ps to ensure uncorrelated time averages. In this way, isothermal plots of the CN vs. P can be used to investigate the melt structure as density (or pressure) changes along an isotherm. Coordination numbers of Si, Mg, and O around a central O, and oxygen coordinated around central Si and Mg atoms were determined at each state point and are given in Figures 7 and 8 at 3500 and 5000 K as a function of pressure. CN statistics are presented as percentages of the number fraction.

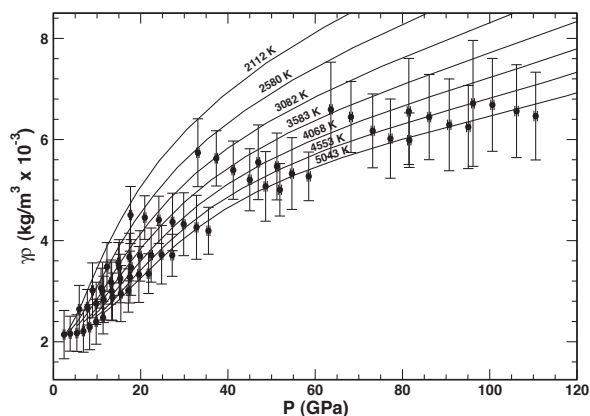


FIGURE 6. The product of the thermodynamic Grüneisen parameter and liquid density ($\gamma\rho$) plotted vs. pressure. The non-zero slopes of the MD data arrayed along each isochore show that the simple integrated form of the Mie-Grüneisen EOS requiring constancy of $\gamma\rho$ is only approximately applicable. MD simulation data are shown with estimated uncertainties. Curves are calculated from the model developed in the appendix. Isotherms are chosen as average temperatures of the simulations.

Oxygen as central atom. By atom number and volume, Mg_2SiO_4 is 57 and 86% oxygen, respectively. It is logical therefore to consider the CN values of Si, Mg, and O around central O atoms. In Figure 7a, the coordination of Si around central oxygen is shown at 3500 and 5000 K as a function of pressure. At low pressure, ~60% of the oxygen has one nearest Si neighbor, whereas about 20% of the O is “free” oxygen (no closest Si neighbors, CN = 0) and 20% of the oxygen has CN = 2 with respect to Si. The fraction of “free” oxygen (CN = 0) expectedly decreases with increasing pressure. The fraction of CN = 0 oxygen is high, indicating a relatively “defect-ridden” melt structure consistent with depolymerization. As pressure increases, the fraction of non-bridging oxygen (CN = 1) and “free” oxygen (CN = 0) decreases, whereas the fraction of oxygen with two nearest Si neighbors (CN = 2) increases, as does the oxygen of CN = 3. The stoichiometry indicates that as pressure increases, free oxygen (CN = 0) combines with two non-linked tetrahedra (each with CN = 1) to form a tetrahedral dimer in which one oxygen is shared by two Si. At 80 GPa, the fraction of dimers is about 40%, in agreement with Sen and Tangeman (2008) who used MD simulations of Mg_2SiO_4 liquid at 2273 K and the NMR spectrum of ^{29}Si in Mg_2SiO_4 glass to estimate a dimer (Si_2O_7) fraction of 40%. The number of oxygen with three nearest neighbor Si increases from a negligible amount to about 10% at 97 GPa. The average CN increases from slightly above unity at low pressure to about 1.44 at the highest pressure studied. Comparison of results at 3500 and 5000 K indicates that temperature exerts a very weak influence on Si around O coordination statistics; pressure is far more important. The computed increase in shear viscosity of molten Mg_2SiO_4 found using the Green-Kubo method (see below) is consistent with increased polymerization as pressure increases in molten Mg_2SiO_4 .

The coordination of Mg around oxygen is shown in Figure 7b at 3500 and 5000 K. At low pressure, the average coordination number (CN_{avg}) of Mg around O is ~3; as pressure increases so does CN_{avg} to ~3.6. The higher CN for Mg compared to Si around oxygen reflects the large size of Mg relative to Si. The steepest change in Mg CN occurs in the range 10–30 GPa. Similar to Si coordination around O, the effect of increasing temperature from 3500 to 5000 K is weak; the pressure dominates over temperature and exerts a first-order effect on short-range order in molten Mg_2SiO_4 .

In Figure 7c, the CN of oxygen around oxygen is shown. At low pressures, high coordination oxygen polyhedra predominate; CN_{avg} is ~11. There is a small but statistically significant increase in the fraction of CN = 13 and 14, a correlative decrease in CN equal to 9, 10, 11, and 12 near 14 GPa at 3500 K, and an analogous but more poorly defined feature at 5000 K. At pressures greater than about 50 GPa, the abundance of highly coordinated oxygen (CN = 12, 13, and 14) drops off, whereas the oxygen coordinated with 9 or 10 oxygen atoms increases in concentration at both 3500 and 5000 K, although the effect is somewhat muted at 5000 K.

Silicon and magnesium as central atoms. The coordination of oxygen around a central Si gives direct information regarding the local state of polymerization of a melt. Figure 8a shows the CN of oxygen around a central Si atom at 3500 and 5000 K. At relatively low pressure, more than 75% of the Si is tetrahedrally

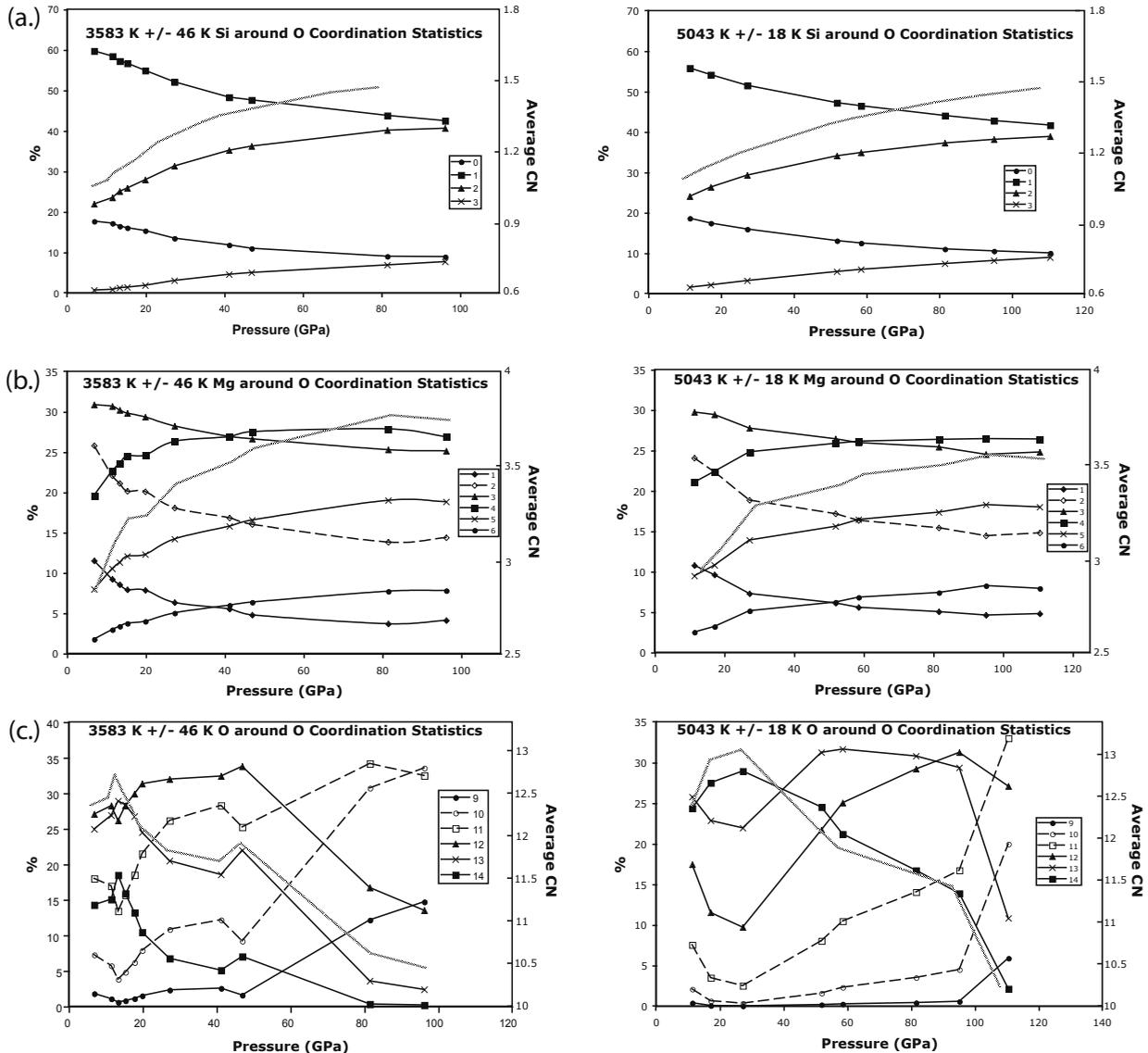


FIGURE 7. (a) Si around O coordination statistics along 3583 and 5043 K isotherms. (b) Mg around O coordination statistics along 3583 and 5043 K isotherms. (c) O around O coordination statistics along 3583 and 5043 K isotherms. The solid thick line represents the average coordination state (CN_{avg}) based on the number fractions.

coordinated with oxygen, the rest mainly in fivefold coordination defining distorted trigonal bipyramidal polyhedra. There is a rapid change in coordination as pressure increases. At ~ 20 GPa, the abundances of fourfold and fivefold Si are equal ($\sim 45\%$) and 10% of the Si is in octahedral (CN = 6) coordination. The abundance of CN = 5 peaks at ~ 30 GPa; the abundance of CN = 5 and 6 are equal (45%) at 43 GPa. At high pressure, the melt is dominated by CN = 6 with very little tetrahedral oxygen and about 15% CN = 5. There is also about 10% of CN = 7. Trends are rather systematic and smooth. These relationships are preserved at 5000 K, although distributions are somewhat broader than at 3500 K and the CN = 5 to 6 crossover occurs at higher pressure, around 60 GPa.

Finally, in Figure 8b the coordination number of oxygen around Mg is shown at 3500 and 5000 K. At low pressure, CN_{avg}

≈ 5.5 . As pressure increases the average CN increases (~ 7.5) near 100 GPa. Octahedrally coordinated Mg attains a maximum at about 20 GPa and decreases systematically as pressure increases. The number of seven-coordinated polyhedra maximize at about 50 GPa, whereas Mg with eight nearest oxygen neighbors attains a maximum at circa 100 GPa. Once again, relations at 5000 K are quite similar except that abundance distributions are somewhat broader.

These observations of the P - T dependence of the CN values of Si and Mg are broadly consistent with the DFT MD study of de Koker et al. (2008).

Transport properties

Self-diffusivity. Self-diffusion coefficients (D) were computed for all runs using accumulated statistics and the

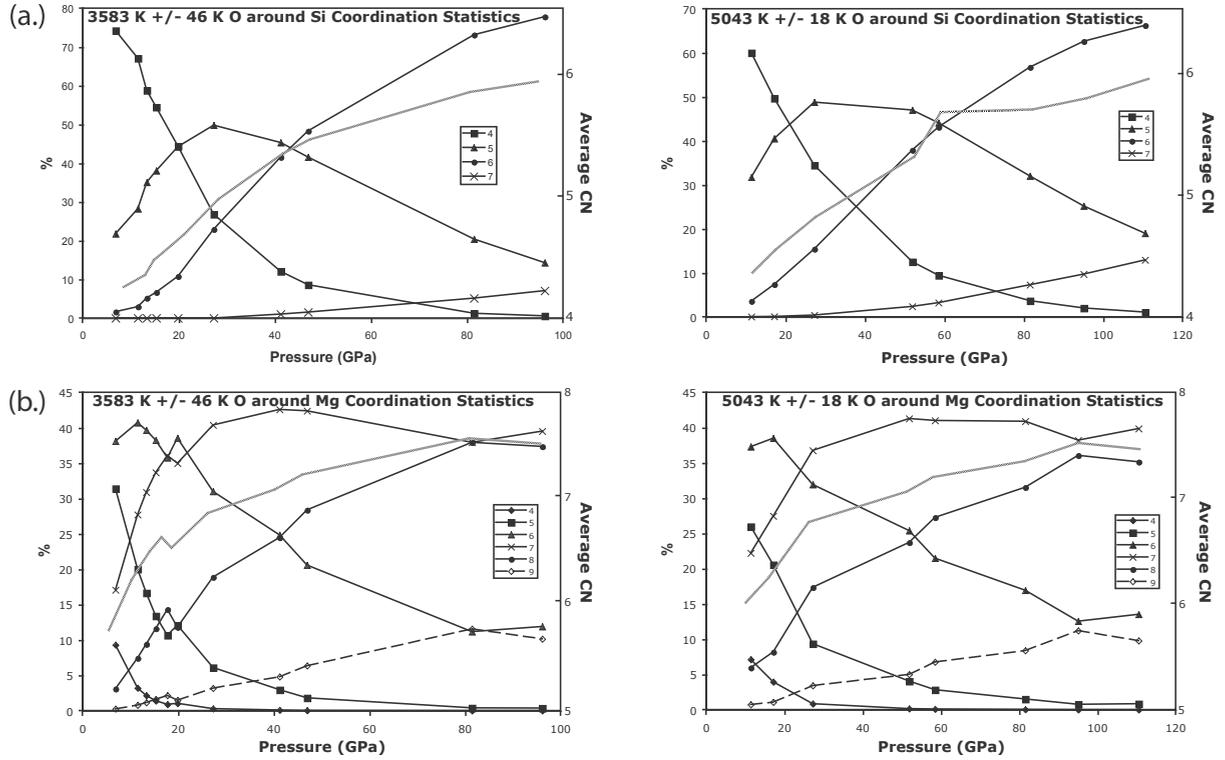


FIGURE 8. (a) Oxygen around Si coordination statistics along 3583 and 5043 K isotherms. (b) Oxygen around Mg coordination statistics along 3583 and 5043 K isotherms. The solid thick line represents the average coordination number, CN_{avg} .

Einstein relation:

$$D_i = \lim_{t \rightarrow \infty} \frac{\left\langle \sum_i^{N_i} [r_i(t) - r_i(0)]^2 \right\rangle}{6N_i t} \quad (5)$$

where r_i is the position of atom i and N_i is the number of atoms of type i . The term in angled brackets, the mean-squared displacement (MSD), is calculated for each state point simulation from atom trajectories. These MSD plots are very linear in time; the Fickian diffusion coefficient is readily calculated from the slope. The very early ballistic part of the MSD (approximately the first 100 fs) is disregarded in the calculation of D .

Self-diffusivities for Mg, Si, and O at all state points are listed in Table 2¹. Self-diffusivities for all atoms at 3583 K for pressure in the range 0–100 GPa are shown in Figure 9. Magnesium remains the most mobile species throughout all P - T space. Oxygen and Si are the slower diffusers. There is a decrease in all diffusivities with increasing pressure along an isotherm. The slope in these coordinates is directly related to the activation volume.

The MD data are well fit by a modified Arrhenian transport model. The expression is:

$$D = D_0 \exp\left(\frac{-(E^* + [V_0^* + V_1^* P])}{RT}\right) \quad (6)$$

where R is the gas constant, E^* is the activation energy for diffusion, V_0^* is the activation volume at zero pressure, and V_1^* is the pressure-derivative of the activation volume for diffusion. Values and statistics computed by regression for E^* , D_0 , and V_1^* are collected in Table 4. Other parameterizations, such as allowing for temperature dependence of the activation volume, do not improve the fit. Activation volume depends principally on pressure ($R^2 > 0.98$ for Mg, Si, and O). Activation energies are in the range 67–79 kJ/mol, with Mg exhibiting the lowest activation barrier. The zero pressure activation volume, V_0^* , is in the range 1.1–1.4 cm^3/mol and is largest for Mg and smallest for Si; for each GPa of pressure increase the activation volume decreases by $\sim 0.005 \text{ cm}^3/\text{mol}$ for Mg and ~ 0.003 for Si (i.e., $V_1^* = -2.6 \times 10^{-3} \text{ cm}^3/\text{mol GPa}$). The atom with the largest zero-pressure activation volume (Mg) also possesses the largest pressure-derivative of the activation volume (V_1^*), an activation volume compensation effect.

Shear viscosity. The shear viscosity was calculated at pressures spanning 7–30 GPa and temperatures 3000–4000 K using the Green-Kubo formulation following the procedures of Nevins and Spera (2007). Long simulations, up to 2 ns, were required for acquisition of robust statistics. In the Green-Kubo method, the temporal decay of the five independent stress auto-correlation functions are related to the dynamical relaxation time and hence the shear viscosity. Viscosity isotherms are shown in Figure 10. The shear viscosity increases with increasing pressure along an isotherm and decreases with increasing temperature along an isobar. At any temperature, the viscosity increases by a factor

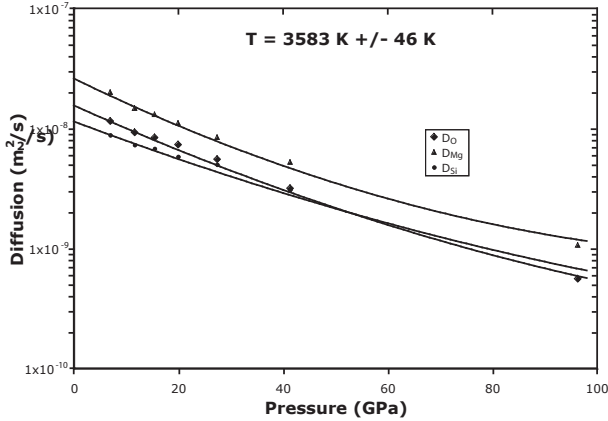


FIGURE 9. Self-diffusivity for O, Mg, and Si at 3583 K vs. pressure. Points represent values derived from MD simulations and curves are based on fit using Equation 6 and parameters from Table 4. The non-linear slope implies a small pressure-dependence of the activation volume for diffusion for all atoms.

of 10 per 70 GPa increase in pressure. Multiple linear regression was used to determine the activation energy (E_{η}^*) and activation volume (V_{η}^*) for viscous flow. The modified Arrhenian expression fits the data well. Its form is:

$$\eta = \eta_0 \exp\left(\frac{E_{\eta}^* + [V_{\eta_0}^* + V_{\eta}^* P]}{RT}\right) \quad (7)$$

quite similar to Equation 6. In general, the activation energies and volumes for diffusion and viscous flow are independent. The parameters of the fit are given in Table 4. Although some work has been done recently on using non-Arrhenian models to describe viscosity in silicate melts (e.g., Russell et al. 2003), our correlation coefficient of $R^2 = 0.998$ indicates the modified Arrhenian form is an excellent model. This is likely due to the temperatures of these simulations being well above the glass transition temperature.

Interestingly, the activation energy for viscous flow is slightly more than half that for self-diffusion of Mg, Si, and O. This observation suggests that cooperative mobility of Mg, Si, and O may be important as a viscous flow mechanism. Careful examination of tagged particle dynamics (not attempted in this study) is needed to better understand the differences in the activation energy for diffusion (E^*) and viscous flow (E_{η}^*). In contrast, the activation volume for viscous flow is almost equal to that for self-diffusion, falling between the comparable values

TABLE 4. Parameters for self-diffusivities of O, Mg, and Si are based on Equation 5 in text; shear viscosity is based on Equation 6

	E^* (kJ/mol)	V_0^* (cm^3/mol)	V_{η}^* [$\text{cm}^3/(\text{mol}\cdot\text{GPa})$]	D_0 (m^2/s) or η_0 (Pa s)	R^2
O	75.636	1.315	-3.375E-03	2.089E-07	0.988
Mg	66.530	1.421	-5.046E-03	2.561E-07	0.988
Si	79.246	1.103	-2.584E-03	1.739E-07	0.980
viscosity	41.018	1.455	-4.777E-03	4.549E-04	0.998

Notes: Numerical values for E^* and V^* in the table are given in rational units for ease of interpretation. Note that numerical values should be converted to SI units (m^3 for volume, J for energy, and Pa for pressure) when computing values at specific P - T points. No unit conversions are required for the pre-exponential terms D_0 and η_0 .

for O and Mg. The shear viscosity of molten Mg_2SiO_4 at 4000 K increases by a factor of 20 as pressure increases from 1 bar (10^{-4} GPa) to 100 GPa.

Self-diffusion and viscous flow. Because self-diffusivity and shear viscosity are computed independently, the data can be used to test the validity of the Stokes-Einstein (SE) and related Eyring (EY) relations between self-diffusion, shear viscosity, and characteristic size of the mobile species.

The SE relation relates the mobility of an atom (i.e., Mg, Si, or O) to the frictional force exerted on the atom as it diffuses through a continuum medium of viscosity η . The model is often used to estimate self-diffusivity when shear viscosity is known or vice versa. In the model, the hydrodynamical friction factor of a spherical “particle” is $f = 6\pi\eta a$ (no slip boundary) or $f = 4\pi\eta a$ (slip boundary), where a is the radius of the diffusing particle. The friction factor is related to the self-diffusion coefficient according to $f = kT/D$, where k is the Boltzmann constant. Equating friction factors gives a relationship between melt viscosity, self-diffusivity, and particle size. For a simple SE fluid, the expression is:

$$a = \frac{kT}{6\pi D\eta} \quad (8a)$$

for no slip boundary condition and

$$a = \frac{kT}{4\pi D\eta} \quad (8b)$$

when slip conditions prevail. Implicit in the constancy of a in Equation 8 is that the P - T dependence of the shear viscosity and the self-diffusivity of oxygen precisely offset one another and that the size of the diffusing “species” is constant.

In Figure 11, the Stokes-Einstein characteristic length is plotted vs. pressure for Mg, Si, and O at 3000 and 5000 K. If the SE expression is valid, then the data should define a trend with zero slope and characteristic lengths should approximately equal the ionic radii of Mg, Si, or O. In fact, the slopes are near zero with very slight dependence upon pressure, agreeing with the SE expectation. Comparing isotherms at low and high tem-

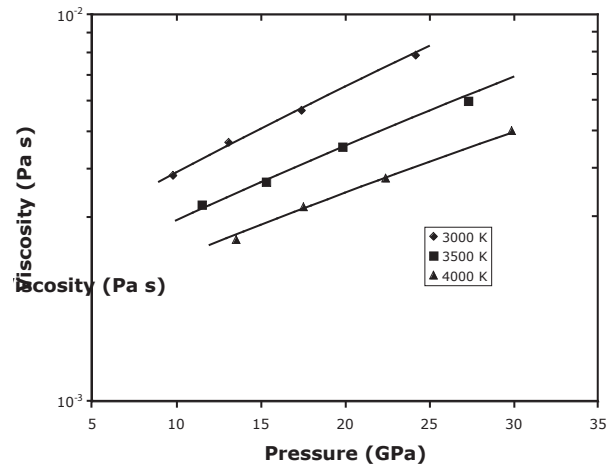


FIGURE 10. Viscosity computed by Green-Kubo method vs. pressure at 3000–4000 K. Points are from MD simulations; curves represent Arrhenian fits based on Equation 7 and Table 4.

peratures shows little dependence on temperature. Moreover, the size parameter for each species is correct within a factor of two if we identify the characteristic length as the ionic radius of the appropriate ion. That is, values of the characteristic length for O, Mg, and Si from Figure 11 are roughly 1.4, 0.85, and 1.5 Å, and compare reasonably well to the ionic radii of 1.26, 0.86, and 0.54 Å. The only anomaly is in the ordering; one would expect $a_{\text{O}} > a_{\text{Mg}} > a_{\text{Si}}$, whereas from Figure 11, $a_{\text{Si}} > a_{\text{O}} > a_{\text{Mg}}$. This anomaly may signify that Si does not diffuse independently of oxygen but instead Si mobility depends cooperatively on oxygen motion.

The Eyring model is similar to the SE model although it is based on a somewhat more detailed atomic level picture (e.g., Eyring 1982). Applied to molten Mg_2SiO_4 , the relationship between self-diffusivity and viscosity is:

$$\frac{kT}{(V/nN_A)^{1/3}D\eta} = \xi \quad (9)$$

where n is the number of atoms per formula unit ($n = 7$), $V(P, T)$ is the molar volume at the state point at which the atom diffusivity and shear viscosity are evaluated, and N_A is Avogadro's number. In a simple fluid, such as liquid argon for example, ξ represents the number of nearest neighbors surrounding a central diffusing atom that are pushed aside during the atom hopping event. In other words, ξ represents the number of atoms in the activated complex. Typically, ξ takes on values in the range 6–12 in simple fluids. If we consider molten Mg_2SiO_4 as essentially an oxygen superlattice held together by high field strength Si, values of ξ within the range of the CN_{avg} of O around central Si (~ 5 –6, Fig. 7) and the CN_{avg} of O around O (~ 12 , Fig. 8), one might expect a value of ξ around 10. In this admittedly simplistic view, melt is pictured as an oxygen superlattice that governs the kinetics of flow and atom mobility. This notion is not exactly correct, of course, but seems like a reasonable first-approximation. In Figure 12, computed values of ξ are shown for several isotherms as a function of pressure. The values of ξ for O and Si are around 8, which is broadly consistent with the coordination statistics of Figures 7 and 8. In light of the crudity of the Stokes-Einstein and Eyring models applied to structured molten silicates, the broad agreement between MD results and these elementary mechanistic theories is surprisingly good. Whether this is coincidental can only be better appreciated by applying the theory to other compositions.

CONCLUDING REMARKS

We carried out pair-potential MD simulations of liquid Mg_2SiO_4 along 12 isochores at 63 state points between 2100–5000 K and 2–110 GPa using the transferable potential model of Matsui (1998). The MD results were used to compute the thermal pressure, isobaric expansivity, isothermal compressibility, isochoric heat capacity, Grüneisen parameter, and the internal energy of molten Mg_2SiO_4 over a range of conditions corresponding to the Earth's mantle. Values are compiled in Table 3¹ at all MD state points. An EOS and a self-consistent thermodynamic model have been developed from these data. The model is based upon the Universal EOS of Vinet et al. (1986, 1987, 1989) and the potential energy scaling relation of Rosenfeld and Tarazona (1998). A crystal-liquid density cross-over near 15 GPa at 2100

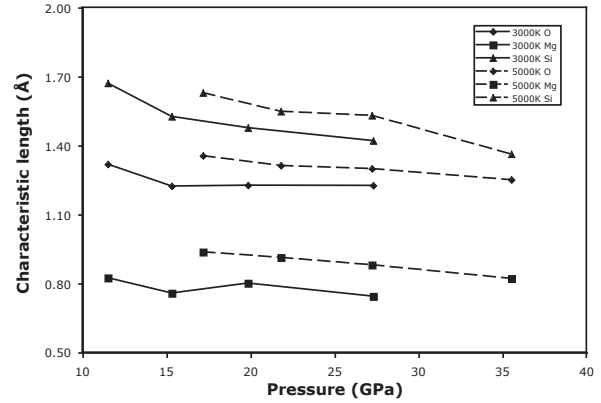


FIGURE 11. Stokes-Einstein plot based on Equation 7b for O, Si, and Mg at 3000 and 5000 K vs. pressure. The ordinate is the length scale a equivalent to the effective hydrodynamic radius of the diffusing particle. a is approximately constant, consistent with the SE relation. For oxygen, the characteristic length closely approximates the ionic radius of oxygen.

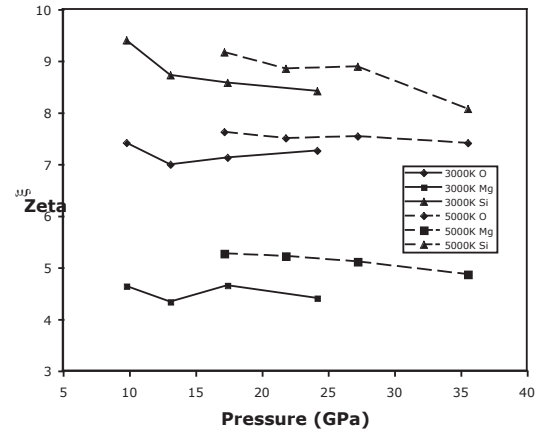


FIGURE 12. Parameter ξ , related to the number of neighboring atoms the diffusing entity must push aside to allow flow vs. pressure based on the Eyring relationship, Equation 9. The lack of significant pressure-dependence of ξ is consistent with the expectation from the Eyring model. Values of ξ around 6–10 are expected based on coordination statistics from the MD simulations.

K is predicted. The ratio of the Grüneisen parameter to the molar volume is not constant as demanded by the simple integrated form of the Mie-Grüneisen EOS but instead varies by $\sim 20\%$ over the temperature range 2000–5000 K.

Profound changes in melt structure at the atomic level take place in response to increasing pressure. Temperature effects, although present, are much less important. For example, along the 3500 K isotherm, the fraction of Si (IV), Si (V), and Si (VI) first-coordination polyhedra changes from 78, 20, and 2% at 5 GPa to 1, 18, and 80%, respectively, at 95 GPa. The abundance of fivefold oxygen present attains a maximum at ~ 30 GPa at 3500 K. Oxygen packing around central Mg follows similar trends although the mean coordination number is higher with Mg (IV) and Mg (VI) decaying monotonically with increasing pressure. Mg (VI) attains a maximum at 20 GPa and Mg (VII)

and Mg (VIII) increase monotonically with increasing pressure. The mean CN of O around Mg of ~ 5.5 at low P increases to ~ 7.5 at 90 GPa. The packing of Si around central oxygen also shows systematic changes with increasing pressure. At $P \sim 5$ GPa, 60% of the Si has one nearest O neighbor, whereas 20% of the Si has either two (Si_2O_7 dimer) or no oxygen as a nearest neighbor. Polymerization occurs as pressure increases as two SiO_4 tetrahedra condense to form a dimer and produce free oxygen. Hence at 5 GPa, 80% of the oxygen is non-bridging oxygen (NBO) and the fraction of bridging oxygen (BO) is $\sim 20\%$. In contrast, at 90 GPa about equal amounts of BO and NBO coexist. The mean CN of Mg around central oxygen shows relatively little variation except for a modest increase from ~ 3 to ~ 3.6 in the pressure range 5–100 GPa at 3500 K. In contrast, the coordination of oxygen around other oxygen reveals two interesting features. The mean CN of O around O at low P (5 GPa) is ~ 11.5 with O (XI), O (XII), and O (XIII) dominating. At P corresponding to the crystalline polymorphic inversion of olivine to β -spinel structure, the abundance of O (IX), O (X), O (XI), and O (XII) all decrease abruptly, whereas O (XIII) and O (IVX) increase in abundance. At about 40 GPa O (IX) and O (X) increase such that the mean CN at 100 GPa is ~ 10 , lower than the mean oxygen around oxygen CN at 5 GPa.

Self-diffusivities for Si, Mg, and O are fit to a modified Arrhenian expression and exhibit monotonic decrease along an isotherm. Activation energies are in the range 67–79 kJ/mol with Mg exhibiting the lowest activation barrier. The zero pressure activation volume V^* is in the range 1.1–1.4 cm^3/mol and is largest for Mg and smallest for Si consistent with ionic radii. The shear viscosity was computed using the Green-Kubo formulation and MD values for the temporal decay of the off-diagonal components of the stress tensor. The shear viscosity follows the modified Arrhenian expression with an activation energy for viscous flow of 41 kJ/mol and a zero-pressure activation volume of 1.5 cm^3/mol , essentially identical to the activation volume for diffusion. The validity of the Stokes-Einstein and Eyring models for relating self-diffusion to shear viscosity have been tested and show reasonable congruity. Data from the MD simulations are used to develop a comprehensive EOS for molten Mg_2SiO_4 . Although the Matsui (1998) potential used is a transferable potential and was not developed specifically for Mg_2SiO_4 we were able to use it to develop an EOS model that reproduces the E - V - P - T relations from simulations very well, and reproduce many properties of the liquid found in the single-composition potential and ab initio studies mentioned.

ACKNOWLEDGMENTS

Support for this investigation was provided by the National Science Foundation (EAR-0609680 to M.S.G. and NSF/ITR-0428774 to F.J.S.). This is OFM Research publication no. 10 and Institute for Crustal Studies Publication no. 2316. Support from the Regents of the University of California is warmly acknowledged. Two anonymous reviewers provided valuable critical commentary.

REFERENCES CITED

Aasland, S. and Macmillan, P.F. (1994) Density-driven liquid-liquid phase separation in the system Al_2O_3 - Y_2O_3 . *Nature*, 369, 633–636.
 Anderson, D. (2007) *New Theory of the Earth*, 384 p. Cambridge University Press, New York.
 Anderson, O.L. (1979) Evidence supporting the approximation $\gamma\rho = \text{const}$ for the Grüneisen parameter of the Earth's lower mantle. *Journal of Geophysical Research*, 84, 3537–3542.

Belonoshko, A.B. and Dubrovinsky, L.S. (1996) Molecular and lattice dynamics study of the MgO-SiO_2 system using a transferable interatomic potential. *Geochimica et Cosmochimica Acta*, 60, 1645–1656.
 Birch, F. (1952) Elasticity and constitution of the Earth's interior. *Journal of Geophysical Research*, 57, 227–286.
 Debenedetti, P. (1996) *Metastable Liquids: Concepts and Principles*. Princeton University Press, New Jersey.
 de Koker, N.P., Stixrude, L., and Karki, B.B. (2008) Thermodynamics, structure, dynamics, and freezing of Mg_2SiO_4 liquid at high pressure. *Geochimica et Cosmochimica Acta*, 72, 1427–1441.
 Eyring, H. (1982) *Statistical Mechanics and Dynamics*, 2nd edition, 785 p. Wiley, New York.
 Ghiorso, M.S. (2004) An EOS for silicate melts. III. Analysis of stoichiometric liquids at elevated pressure: shock compression data, molecular dynamics simulations and mineral fusion curves. *American Journal of Science*, 304, 752–810.
 Lacks, D.J., Rear, D.B., and van Orman, J.A. (2007) Molecular dynamics investigation of viscosity, chemical diffusivities and partial molar volumes of liquids along the MgO-SiO_2 join as functions of pressure. *Geochimica et Cosmochimica Acta*, 71, 1312–1323.
 Lay, T., Garnero, E.J., and Williams, Q. (2004) Partial melting in a thermo-chemical boundary layer at the base of the mantle. *Physics of the Earth and Planetary Interiors*, 146, 441–467.
 Matsui, M. (1998) Computational modeling of crystals and liquids in the system $\text{Na}_2\text{O-CaO-MgO-Al}_2\text{O}_3\text{-SiO}_2$. In M.H. Manghni and T. Yagi, Eds., *Properties of Earth and Planetary Materials at High Pressure and Temperature*, p. 145–148. Geophysical Monograph Series, AGU, Washington, D.C.
 McQuarrie, D.A. (2000) *Statistical Mechanics*. University Science Books, New York.
 Mosenfelder, J.L., Asimov, P.D., and Ahrens, T.J. (2007) Thermodynamic properties of Mg_2SiO_4 liquid at ultra-high pressures from shock experiments to 200 GPa on forsterite and wadsleyite. *Journal of Geophysical Research: Solid Earth*, 112, B06208.
 Nevins, D. and Spera, F.J. (2007) Accurate computation of shear viscosity from equilibrium molecular dynamics simulations. *Molecular Simulation*, 33, 1261–1266.
 ——— (2009) *Understanding silicate geoliquids at high temperature and pressures through molecular dynamics simulations*. Dissertation, University of California, Santa Barbara.
 Philpotts, A.R. (1976) Silicate liquid immiscibility: its probable exponent and petrogenetic significance. *American Journal Science*, 276, 1147–1177.
 Poirier, J.P. (2000) *Introduction to the Physics of the Earth's Interior*, 2nd edition, 312 p. Cambridge University Press, U.K.
 Quarenii, F. and Mulargia, F. (1988) The validity of the common approximate expressions for the Grüneisen parameter. *Geophysical Journal International*, 93, 505–519.
 Roedder, E. (1951) Low-temperature liquid immiscibility in the system $\text{K}_2\text{O-FeO-Al}_2\text{O}_3\text{-SiO}_2$. *American Mineralogist*, 36, 282–282.
 Rosenfeld, Y. and Tarazona, P. (1998) Density functional theory and the asymptotic high density expansion of the free energy of classical solids and fluids. *Molecular Physics*, 95, 141–150.
 Russell, J.K., Giordano, D., and Dingwell, D.B. (2003) High-temperature limits on viscosity of non-Arrhenian silicate melts. *American Mineralogist*, 88, 1390–1394.
 Saika-Voivid, I., Soiertino, F., and Pool, P.H. (2000) Computer simulations of liquid silica: Equation of state and liquid-liquid phase transition. *Physical Review E*, 63, 011202.
 Sen, S. and Tangeman, J. (2008) Evidence for anomalously large degree of polymerization in Mg_2SiO_4 glass and melt. *American Mineralogist*, 93, 946–949.
 Senker, J. and Rossler, E. (2001) Triphenyl phosphate: a candidate for liquid polymorphism. *Chemical Geology*, 174, 143–156.
 Skibinsky, A., Buldyrev, S.V., Franzese, G., Malescio, G., and Stanley, H.E. (2004) Liquid-liquid phase transitions for soft-core attractive potentials. *Physical Review E*, 69, 061206.
 Tanaka, H. (2000) General view of a liquid-liquid phase transition. *Physical Review E*, 62, 6968–6976.
 Vinet, P., Ferrante, J., Smith, J.R., and Rose, J.H. (1986) A universal equation of state for solids. *Journal of Physics C: Solid State Physics*, 19, L467–L473.
 Vinet, P., Smith, J.R., Ferrante, J., and Rose, J.H. (1987) Temperature effects on the universal equation of state of solids. *Physical Review B*, 35, 1945–1953.
 Vinet, P., Rose, J.H., Ferrante, J., and Smith, J.R. (1989) Universal features of the equation of state of solids. *Journal of Physics: Condensed Matter*, 1, 1941–1963.